Microstructure and Dielectric Properties of Piezoelectric Magnetron Sputtered w-$Sc_xAl_{1-x}N$ thin films

Agnė Žukauskaitė, Gunilla Wingqvist, Justinas Previous Pališaitis, Jens Jensen, Per O. Å. Persson, Ramin Matloub, Paul Muralt, Yunseok Kim, Jens Birch and Lars Hultman

Linköping University Post Print

N.B.: When citing this work, cite the original article.

Original Publication:

Agnė Žukauskaitė, Gunilla Wingqvist, Justinas Pališaitis, Jens Jensen, Per O. Å. Persson, Ramin Matloub, Paul Muralt, Yunseok Kim, Jens Birch and Lars Hultman, Microstructure and Dielectric Properties of Piezoelectric Magnetron Sputtered w-$Sc_xAl_{1-x}N$ thin films, 2012, Journal of Applied Physics, (111), 9, 093527.
http://dx.doi.org/10.1063/1.4714220
Copyright: American Institute of Physics (AIP)
http://www.aip.org/

Postprint available at: Linköping University Electronic Press
http://urn.kb.se/resolve?urn=urn:nbn:se:liu:diva-76471

JOURNAL OF APPLIED PHYSICS 111, 093527 (2012)

Microstructure and dielectric properties of piezoelectric magnetron sputtered w-$Sc_xAl_{1-x}N$ thin films

Agne Zukauskaite,[1] Gunilla Wingqvist,[1] Justinas Palisaitis,[1] Jens Jensen,[1] Per O. Å. Persson,[1] Ramin Matloub,[2] Paul Muralt,[2] Yunseok Kim,[3] Jens Birch,[1] and Lars Hultman[1]

[1]*Thin Film Physics Division, Department of Physics, Chemistry, and Biology (IFM), Linköping University, SE-581 83 Linköping, Sweden*
[2]*Ceramics Laboratory, Ecole Polytechnique Fédérale de Lausanne EPFL, Lausanne, Switzerland*
[3]*Center for Nanophase Materials Sciences, Oak Ridge National Laboratory, Oak Ridge, Tennessee 37831, USA*

(Received 14 February 2012; accepted 6 April 2012; published online 9 May 2012)

Piezoelectric wurtzite $Sc_xAl_{1-x}N$ (x = 0, 0.1, 0.2, 0.3) thin films were epitaxially grown by reactive magnetron co-sputtering from elemental Sc and Al targets. Al_2O_3(0001) wafers with TiN(111) seed and electrode layers were used as substrates. X-ray diffraction shows that an increase in the Sc content results in the degradation of the crystalline quality. Samples grown at 400 °C possess true dielectric behavior with quite low dielectric losses and the leakage current is negligible. For ScAlN samples grown at 800 °C, the crystal structure is poor and leakage current is high. Transmission electron microscopy with energy dispersive x-ray spectroscopy mapping shows a mass separation into ScN-rich and AlN-rich domains for $x \geq 0.2$ when substrate temperature is increased from 400 to 800 °C. The piezoelectric response of epitaxial $Sc_xAl_{1-x}N$ films measured by piezoresponse force microscopy and double beam interferometry shows up to 180% increase by the addition of Sc up to x = 0.2 independent of substrate temperature, in good agreement with previous theoretical predictions based on density-functional theory. © *2012 American Institute of Physics*.
[http://dx.doi.org/10.1063/1.4714220]

I. INTRODUCTION

There is a growing interest in the tailoring of AlN material's properties. AlN in its stable form is a wide bandgap (6.2 eV) non-ferroelectric piezoelectric polar material that is utilized in opto-electronics and electro-acoustics. Alloys of wurtzite AlN with other wurtzite group III nitrides (GaN (Ref. 1) and InN (Ref. 2)) hold promise for bandgap and lattice parameter engineering in high frequency optical applications. AlN has also been utilized in alloys with cubic (B1) transition metal nitrides (i.e., TiN (Ref. 3) and ZrN (Ref. 4)) to obtain increased mechanical strength. In addition, it is today the dominating choice for the piezoelectric active layer in the thin-film bulk-acoustic resonators (TFBARs) for high-frequency filters in telecommunication applications due to the largest piezoelectric constant ($e_{33} = 1.46\,C/m^2$) among the tetrahedrally bonded binary semiconductors.[5] However, despite chemical and high-temperature stability, high Q values, low acoustic losses, and a good compatibility to thin film technology[6] of AlN, its rather low electromechanical coupling is limiting the bandwidth for potential applications in wide band communication. Therefore, there is a need to further improve the piezoelectric properties of AlN with retained low electrical and acoustic losses.

Experiments demonstrated a 400% increase in piezoelectric modulus d_{33} for $Sc_xAl_{1-x}N$ alloys with x = 0.43.[7] The increase in d_{33} was simulated to be an intrinsic alloying effect related to an increase in piezoelectric constant (e_{33}) as well as a decrease in stiffness constant (c_{33}^E).[8] A theoretical and experimental structural study of $Sc_xAl_{1-x}N$ showed that there is a competition between rocksalt (c-) and wurtzite (w-) structural phases. Both phases have positive mixing enthalpies and are thereby metastable; however, the wurtzite structure was theoretically predicted to be preferred for solid solution with $x < 0.55$.[9]

We have recently reported that by limiting the substrate temperature to 400 °C w-$Sc_xAl_{1-x}N$ ($0 \leq x \leq 0.3$), solid solutions can be produced with pure dielectric properties with only minor increase in the dielectric losses compared to AlN films.[10] Our evidence of generating a dielectric solid solution together with a well-defined extraction of the dielectric constants enabled prediction of increase in electromechanical coupling factor (k_t^2) from 7% to 10% in the range of x = 0–0.2. Independent studies have later confirmed those k_t^2 values by studying $Sc_xAl_{1-x}N$ ($0 < x < 0.15$) TFBAR structures in the 2–2.5 GHz range.[11,12] At growth temperatures higher than 400 °C, increased leakage currents and degradation in structural properties of the w-$Sc_xAl_{1-x}N$ solid solutions are generated.[10] This degradation of the material quality is suggested to be caused by phase instabilities.[10,13]

So far, studies of the ScAlN system were more focused on perovskite-type and cubic phases occurring with the high Sc content.[14] It has been shown that as-deposited cubic $Sc_{0.57}Al_{0.43}N$ is stable up to temperatures of 1000–1100 °C, above which it separates via nucleation and growth at domain boundaries into non-isostructural c-ScN and w-AlN.[15] Additionally, opto-electronic properties of $Sc_xAl_{1-x}N$ nanowires with x = 0.05 were investigated.[16] However, no detailed study on the phase stability and transformations of the technologically interesting Al-rich wurtzite $Sc_xAl_{1-x}N$ thin films was performed.

 © 2012 American Institute of Physics

Downloaded 19 Jun 2012 to 130.236.83.30. Redistribution subject to AIP license or copyright; see http://jap.aip.org/about/rights_and_permissions

Here, we present a systematic experimental study on the growth temperature dependency of the crystal- and microstructure in $Sc_xAl_{1-x}N$ in the range of $0 \leq x \leq 0.3$. Thin films were grown by dual target magnetron sputter epitaxy (MSE), with the substrate at floating potential (no additional bias). The as-deposited film structures were studied in detail with x-ray diffraction and transmission electron microscopy. The dielectric and piezoelectric properties are then presented in correlation to the structural properties.

II. EXPERIMENTAL DETAILS

Thin films of 250–500 nm thickness were prepared by magnetically unbalanced reactive DC magnetron sputtering in an Ar/N discharge in a UHV vacuum system with a base pressure of 6×10^{-7} Pa and process pressure of 0.17 Pa at flows of 30 SCCM Ar and 19.8 SCCM N_2. Two separate elemental 5 cm diameter targets were used: 99.995% pure metallic Al and 99.9995% pure metallic Sc. Growth was done onto previously grown 100–200 nm thick conductive single-crystal TiN(111) seed layers on Al_2O_3(0001) substrates, with growth temperature of 800 °C. $Sc_xAl_{1-x}N$ samples with x = 0, 0.1, 0.2, and 0.3 were grown. During the $Sc_xAl_{1-x}N$ growth, a constant-power mode was used on each cathode, and the relative amounts of Sc and Al were controlled by varying the relative applied power, keeping the total power at 150 W. Before growing the TiN seed layer, the Al_2O_3(0001) substrates were cleaned in ultrasonic baths of trichloroethylene, acetone, and isopropanol and blown dry with N_2. The same cleaning procedure, but without the trichloroethylene treatment, was repeated for the TiN-coated samples prior to the deposition of the ScAlN films. Thermal degassing at the selected substrate temperature was performed for 1 h and the targets were clean-sputtered in Ar for 6 min prior to deposition. The substrate heater temperature was controlled via a thermocouple placed behind the sample and calibration was performed at the TiN surface using a pyrometer. Three different substrate temperatures (T_s) of 400, 600, and 800 °C were selected for the study.

Composition and impurity levels were determined by time of flight energy elastic recoil detection analysis (ToF-E ERDA) using a primary ion beam of 40 MeV $^{127}I^{9+}$ performed at the Tandem Laboratory in Uppsala, Sweden. The crystalline quality was evaluated using a Cu Kα x-ray diffraction (XRD) Philips Bragg-Brentano diffractometer in $\theta/2\theta$ mode. For microstructural analysis, transmission electron microscopy (TEM) and scanning TEM (STEM) with high-angle annular dark field (HAADF), as well as STEM energy dispersive x-ray spectroscopy (EDX) mapping of 20×20 and 25×25 nm areas with 1 nm^2 pixel size were performed in a Tecnai G2 TF20 UT FEG microscope operated at 200 kV. Cross-sectional TEM samples were prepared by mechanical polishing followed by ion milling. The dielectric properties were evaluated through the current-voltage (I–V) measurements in the 0–5 V range that were performed on Au/Cr/$Sc_xAl_{1-x}N$/TiN/Al_2O_3 structures using a probe station equipped with a HP4284A LCR-meter and a Keithley 237 IV-meter. Double-beam interferometry (DBI) and piezoresponse force microscopy (PFM) were used to evaluate piezoelectric properties of the films. In both of the techniques, converse piezoelectric response was measured, that is, how much the material expands/contracts with applied electric voltage. PFM is based on the atomic force microscopy (AFM) instrument, where the piezoelectric displacement response can be measured by applying an electrical voltage very locally with a conductive AFM probe.[17,18] The measurements were performed at Max Planck Institute of Microstructure Physics in Halle, Germany using a XE-100 AFM with a SR830 lock-in amplifier at a 25 kHz frequency in an AC voltage sweep regime from 0 to 4 V; each measurement was repeated 20 times. In the DBI method, the electric voltage was applied onto the top electrodes (600 μm in diameter) and the film thickness change was measured with a double-beam interferometer, where the bending of the substrate is compensated for,[19] and thus able to measure the clamped piezoelectric coefficient $d_{33,f}$ of thin films. The high sensitivity of the method gives results that well correlate with the average response measured with piezo-sensitive AFM imaging.[20]

III. RESULTS AND DISCUSSION

A. Composition of the films

A typical example of a ToF-E ERDA profile for the $Sc_{0.2}Al_{0.8}N$ sample grown at 800 °C is shown in Figure 1. No variations in film composition for the different growth temperatures were found. All samples are stoichiometric with the (Al + Sc)/N ratio being 1 and with levels of Sc and Al being constant throughout the film with accuracy of 3%. No diffusion of Ti from the seed layer can be detected in the bulk of the film. The analysis revealed that films contain traces of F – a common contamination coming from the process of manufacturing the Sc sputter targets. There is an oxide layer on top of the film, but samples contain no more than 1 at. % O throughout the film thickness, and C is below the detection limit. There is also a presence of a heavy element, possibly Ta (not shown in the graph), which also is a common contamination in rare-earth elemental targets.[15] No Ar, a typical contamination in magnetron sputtering processes,[21] is detected, which can be attributed to having no dc bias applied on the samples during the growth as well as

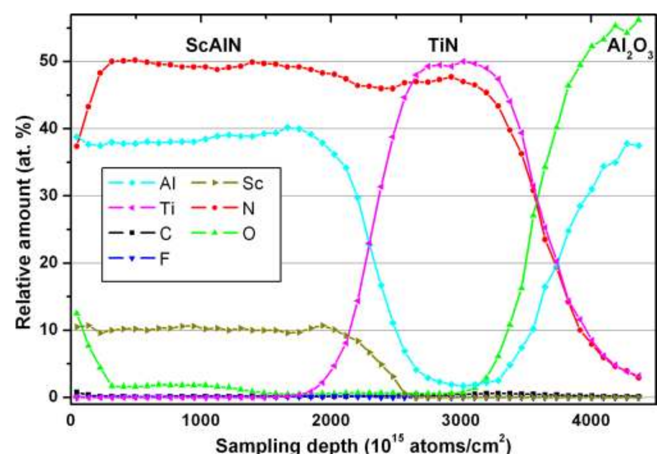

FIG. 1. ToF-E ERDA profile recorded from a typical sample, $Sc_{0.21}Al_{0.79}N$ (1 at. % oxygen, traces of C and F) grown on Al_2O_3 with a TiN seed layer.

Downloaded 19 Jun 2012 to 130.236.83.30. Redistribution subject to AIP license or copyright; see http://jap.aip.org/about/rights_and_permissions

high substrate temperature and the relatively low intensity of fast neutrals being reflected from the Al target.[22,23]

B. Structural properties and influence of the growth temperature

XRD from the $Sc_xAl_{1-x}N$ with $x = 0.2$ and $x = 0.3$ as well as the reference AlN samples deposited at three different temperatures are shown in Fig. 2. for (a) 400 °C, (b) 600 °C, and (c) 800 °C, respectively. The only observed diffraction peaks in the $\theta/2\theta$ scan correspond to wurtzite AlN(0002) or ScAlN(0002), cubic TiN(111) seed layer, and Al_2O_3(0006) substrate. No indications of additional phases or orientations were found. The films are thus c-axis oriented and pole figures (not shown here) confirm epitaxial growth for samples with $x = 0.1$ and $x = 0.2$. With increasing Sc content, the film peak position is shifting towards lower 2θ values, indicating an increase in the out-of-plane lattice constant. This trend corresponds well with previously reported experimental results of lattice constant measurements and theoretical calculations in Ref. 9.

Rocking curve measurements show that TiN films (marked by * in Fig. 2) are highly orientated with full width at half maximum (FWHM) values of the 111 peak $\leq 0.051°$.

According to the peak intensities in $\theta/2\theta$ scans and rocking curve FWHM measurements of the 0002 peaks, the best crystalline quality of the reference AlN thin films (FWHM 0.452) was obtained at $T_s = 800$ °C, which is to be expected due to the higher ad-atom mobility allowing for better epitaxial growth of the stable binary wurtzite phase. However, for the Sc-containing samples, it is seen that with increasing temperature or Sc concentration, the crystalline quality is degraded. $Sc_{0.1}Al_{0.9}N$ (not shown here) and $Sc_{0.2}Al_{0.8}N$ samples still exhibit a decent XRD response when grown at $T_s \leq 600$ °C, but for $Sc_{0.3}Al_{0.7}N$, there are no diffraction peaks originating from the film. For all Sc concentrations discussed, samples deposited at 400 °C exhibit the best results, with a rocking curve FWHM of 1° for the $Sc_{0.2}Al_{0.8}N$ film (Fig. 2(a), $x = 0.2$) and values higher than 2° for $x = 0.3$.

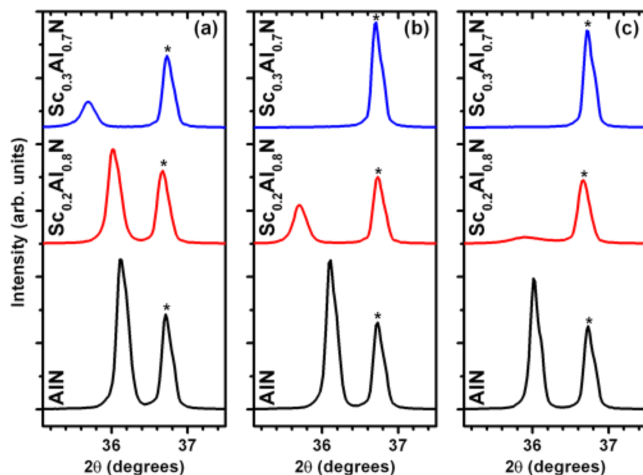

FIG. 2. X-ray diffraction patterns for $Sc_xAl_{1-x}N$ films: AlN (black), $Sc_{0.2}Al_{0.8}N$ (red), and $Sc_{0.3}Al_{0.7}N$ (blue), comparison between different deposition temperatures: (a) $T_s = 400$ °C, (b) $T_s = 600$ °C, and (c) $T_s = 800$ °C. Peaks corresponding to the TiN(111) seed layer are marked by *.

Depositing at lower temperatures provided no improvement in the XRD response and room temperature depositions gave very low diffraction responses for both AlN and ScAlN films.

C. Microstructure and crystal structure

Based on the XRD results, AlN, $Sc_{0.2}Al_{0.8}N$, and $Sc_{0.3}Al_{0.7}N$ films deposited at $T_s = 400$ and 800 °C were selected for the cross-sectional TEM analysis. Dark field (DF) TEM overview micrographs together with selected area electron diffraction (SAED) patterns are displayed in Figure 3. High resolution TEM (HRTEM) images as well as corresponding fast Fourier transforms (FFT) from typically 10×10 nm areas are shown in Figure 4. EDX elemental maps for $Sc_{0.2}Al_{0.8}N$ and $Sc_{0.3}Al_{0.7}N$ are presented in Figure 5.

1. AlN

Analysis of the DF TEM image of the AlN sample grown at 400 °C reveals a film composed of large columnar grains with no well-defined boundaries (Fig. 3(a)). With increased growth temperature, DF TEM analysis of the 800 °C sample shows a dense columnar structure with well-aligned 6–7 nm

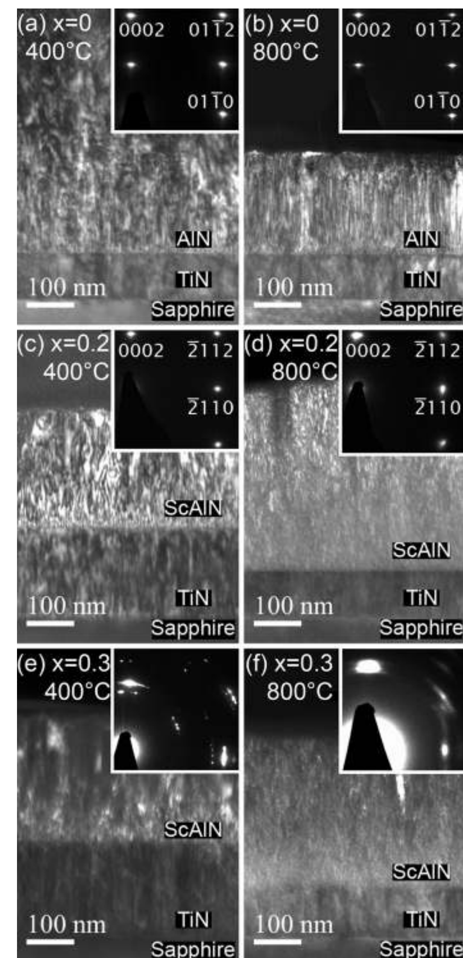

FIG. 3. Dark field TEM micrographs and corresponding SAED patterns (top right corner) of AlN, $Sc_{0.2}Al_{0.8}N$, and $Sc_{0.3}Al_{0.7}N$ films: (a) AlN, $T_s = 400$ °C, (b) AlN, $T_s = 800$ °C, (c) $Sc_{0.2}Al_{0.8}N$, $T_s = 400$ °C, (d) $Sc_{0.2}Al_{0.8}N$, $T_s = 800$ °C, (e) $Sc_{0.3}Al_{0.7}N$, $T_s = 400$ °C, and (f) $Sc_{0.3}Al_{0.7}N$, $T_s = 800$ °C. SAED patterns in (a) and (b) are along the $[2\bar{1}\bar{1}0]$ zone axis, and in (c)–(e) – along the $[01\bar{1}0]$ zone axis.

Downloaded 19 Jun 2012 to 130.236.83.30. Redistribution subject to AIP license or copyright; see http://jap.aip.org/about/rights_and_permissions

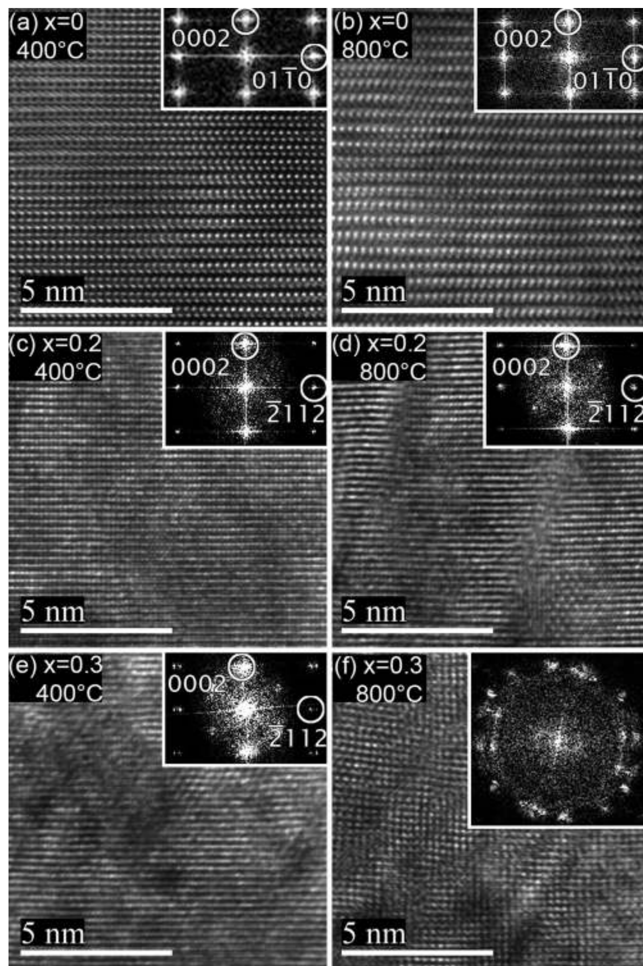

FIG. 4. Cross-section HR-TEM and the corresponding Fast Fourier transform (top right corner) of AlN, $Sc_{0.2}Al_{0.8}N$, and $Sc_{0.3}Al_{0.7}N$ films: (a) AlN, $T_s = 400\,°C$, (b) AlN, $T_s = 800\,°C$, (c) $Sc_{0.2}Al_{0.8}N$, $T_s = 400\,°C$, (d) $Sc_{0.2}Al_{0.8}N$, $T_s = 800\,°C$, (e) $Sc_{0.3}Al_{0.7}N$, $T_s = 400\,°C$, and (f) $Sc_{0.3}Al_{0.7}N$, $T_s = 800\,°C$. In FFT, only spots corresponding to hcp along $[2\bar{1}\bar{1}0]$ zone axis in AlN and along $[01\bar{1}0]$ in ScAlN are indexed, though spots originating from secondary orientation can also be seen in (d) and (e).

wide columnar grains in the growth direction (Fig. 3(b)). SAED patterns along the $[2\bar{1}\bar{1}0]$ zone axis for both AlN films are composed of sharp discrete spots corresponding to wurtzite structure (insets in Figs. 3(a) and 3(b)) confirming single phase as well as high crystalline quality. HRTEM images also reveal that for both AlN films, the crystal structure is well-ordered, independent of growth temperature (Figs. 4(a) and 4(b)). FFT spot patterns from the corresponding HRTEM images (insets in Figs. 4(a) and 4(b)) also show discrete spots corresponding to a single orientation, confirming the XRD and SAED results. As described below, both films perform well in electrical and piezoelectrical measurements; however, it should be noted that increasing the substrate temperature up to $T_s = 800\,°C$ has a positive effect on the AlN quality according to the peak intensity of XRD $\theta/2\theta$ (Fig. 2) and rocking curve FWHM measurements.

2. $Sc_{0.2}Al_{0.8}N$

In the DF TEM overview image of the $T_s = 400\,°C$ sample, Fig. 3(c), the columnar microstructure of $Sc_{0.2}Al_{0.8}N$ appears similar to AlN (Fig. 3(a)). Also, the SAED pattern along the $[01\bar{1}0]$ zone axis consists of sharp diffraction spots (inset in the Fig. 3(c)) as for AlN. A minor degradation of crystalline quality can, however, be seen in HRTEM (Fig. 4(c)), where the irregular contrast indicates lattice distortions with addition of Sc, which is in agreement with the XRD results (Fig. 2(a)). STEM and EDX analysis in Fig. 5(a) show a uniform film with no visible elemental segregation.

In the case of $T_s = 800\,°C$, Fig. 3(d), the DF TEM shows a film composed of narrow crystallites having some columnar tendencies. In the SAED pattern along the $[01\bar{1}0]$ zone axis, a slight spot broadening in the circumferential direction is present indicating a degradation of the microstructure (inset in the Fig. 3(d)). The lattice image in Fig. 4(d) clearly reveals the crystal distortion and stacking faults are seen. The EDX elemental map of this sample exhibits indications of the initial stages of a separation into Sc-rich and Al-rich regions (Fig. 5(b)).

Typical FFT spot patterns are shown as insets in Figs. 4(c) and 4(d). For the 400 °C sample, the pattern is composed of discrete spots corresponding to a single hexagonal close packed (hcp) structure along the $[01\bar{1}0]$ zone axis. In the case of 800 °C, the hcp structure along the $[01\bar{1}0]$ zone axis and traces of a secondary orientation are seen.

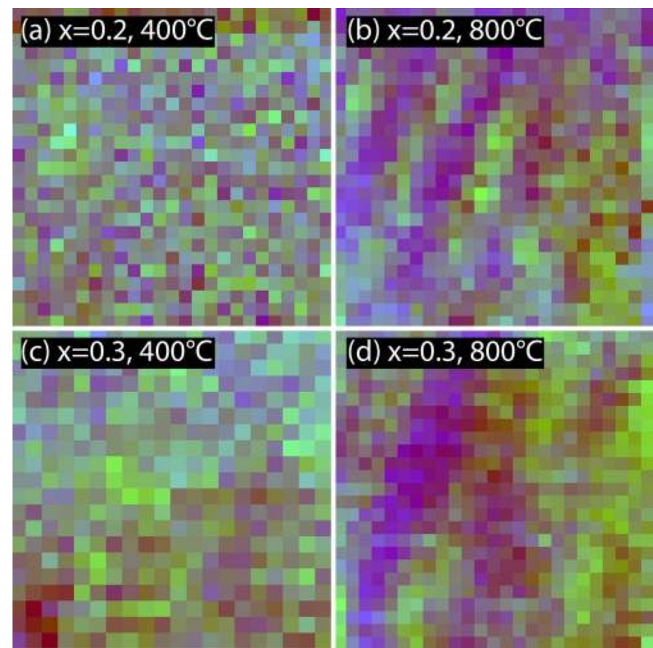

FIG. 5. EDX elemental maps with Sc-rich (green) and Al-rich (dark blue) regions for Sc containing samples (a) $Sc_{0.2}Al_{0.8}N$, $T_s = 400\,°C$, (b) $Sc_{0.2}Al_{0.8}N$, $T_s = 800\,°C$, (c) $Sc_{0.3}Al_{0.7}N$, $T_s = 400\,°C$, and (d) $Sc_{0.3}Al_{0.7}N$, $T_s = 800\,°C$.

3. $Sc_{0.3}Al_{0.7}N$

The DF TEM of $Sc_{0.3}Al_{0.7}N$ film grown at 400 °C, shown in Fig. 3(e), reveals columnar growth and increasing crystallite size with film thickness. The SAED pattern is composed of discrete spots in an arc-like arrangement (inset in the Fig. 3(e)), and the lattice image in Fig. 4(e) shows an increased distortion, resulting from reduced crystal perfection compared to films with lower Sc content. Results from

Downloaded 19 Jun 2012 to 130.236.83.30. Redistribution subject to AIP license or copyright; see http://jap.aip.org/about/rights_and_permissions

EDX elemental mapping are shown in Fig. 5(c), and no clear mass separation could be seen.

$Sc_{0.3}Al_{0.7}N$ film deposited at 800 °C is shown in Fig. 3(f). According to the pronounced and diffused arc pattern in SAED, the film consists of further reduced crystallites with some retained orientation (inset in Fig. 3(f))—with increased growth temperature the overall crystalline quality of the films is degrading. Interestingly, a comparison with the SAED pattern of a sample with x = 0.3 grown at 400 °C (inset in Fig. 3(e)) suggests that the grain size decreases with increased growth temperature. HRTEM analysis shows a highly distorted lattice (Fig. 4(f)). STEM and EDX elemental mapping shows that for $Sc_{0.3}Al_{0.7}N$ grown at 800 °C, there is compositional separation into Sc-rich and Al-rich domains (Fig. 5(d)).

Acquired FFT spot patterns are displayed as insets in Figs. 4(e) and 4(f). For the $T_s = 400$ °C sample, the hcp structure along the $[01\bar{1}0]$ zone axis together with a secondary orientation can be seen, similarly to $T_s = 800$ °C sample with x = 0.2. In the case of 800 °C, a FFT pattern from a larger than 15 × 15 nm area displayed arc-like spots in a ring pattern (inset in Fig. 4(f)). Small randomly oriented grains would explain the drop in intensity in XRD results (Fig. 2(c)).

D. Influence of a seed layer

As it can be seen from DF TEM images in Figs. 3(a)–3(c) and 3(e), films with columnar microstructure exhibited double positioning domain boundaries and threading defects inherited from the TiN seed layer. The lattice mismatch between seed layer and a film is generally an important factor in determining the structural properties. There is a 3.67% in-plane lattice mismatch between the TiN ($d_{(101)} = 3.00$ Å) seed layer and AlN (a = 3.11 Å) films. It has been shown both theoretically and experimentally that alloying AlN with ScN increases the lattice a-parameter, e.g., a = 3.23 Å for $Sc_{0.2}Al_{0.8}N$.[9] This yields an even larger lattice mismatch to the TiN seed layer, which could enhance the degradation in crystalline quality with increased Sc concentrations. Therefore, as an attempt to reduce the defects due to lattice mismatch, $Sc_{0.2}Al_{0.8}N$ and $Sc_{0.3}Al_{0.7}N$ were deposited on previously grown 100 nm thick ZrN seed layers at $T_s = 400$, 600, and 800 °C.

ZrN has a larger in-plane distance ($d_{(101)} = 3.27$ Å) which gives an in-plane mismatch with $Sc_{0.2}Al_{0.8}N$ of only 1.2%. XRD $\theta/2\theta$ scans revealed that the general trend of crystalline degradation with increased Sc content, seen in the case of TiN seed layer, takes place also for the films grown onto ZrN and the expected improvement was not observed. Possible explanations could be a higher surface roughness observed by AFM (not shown here) or a lower ad-atom mobility on ZrN than on TiN, which would have a negative influence on the crystalline quality of ScAlN films despite the better lattice in-plane matching.

E. Electrical properties and influence of the growth temperature

Leakage current through films as a function of applied voltage in the 0–5 V range in $Sc_xAl_{1-x}N$ samples with

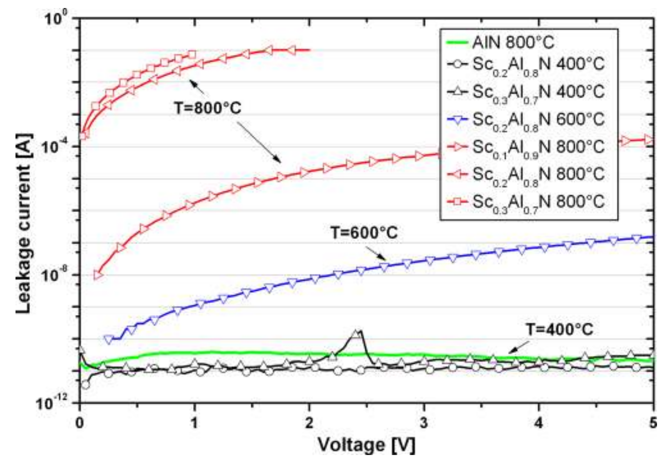

FIG. 6. Leakage currents and their dependence on growth temperature in Sc containing films as comparison to reference AlN sample (solid line).

$T_s = 400$–800 °C and x = 0.1–0.3 is shown in Figure 6. The thickness for all shown films is 250 nm and the Au/Cr top electrodes are 600 μm in diameter. The leakage current in AlN is at the detection limit and independent of growth temperature. Sc-containing samples grown at 400 °C exhibit very low leakage currents comparable to the reference AlN. Capacitance measurements (not shown here) for these low leakage current samples show true dielectric behavior in the frequency range of 1 kHz to 1 MHz. The capacitance versus voltage dependency is also linear, which is expected for oriented polar materials.[24] Reference 10 provides more details on the dielectric properties of the $Sc_xAl_{1-x}N$ films, including the relative dielectric constant ε_r and electromechanical coupling k_t^2.

However, for $T_s > 400$ °C, the leakage currents are high in the ScAlN samples and tend to increase with increasing Sc concentration and growth temperature. The capacitance response is thereby no longer truly dielectric, and obtained non-linear capacitance versus voltage responses indicate that the films contain space charge. The observed dielectrical degradation at high substrate temperature means that structural degradation and phase separation of the films are strong enough to influence not only the crystalline quality but also the dielectric properties of the material. From comparison to the HRTEM results (Figs. 4(a)–4(c) and 4(e)), it can also be noted that for all the samples grown at 400 °C, the HRTEM shows an ordered crystalline structure with minor lattice distortions along with low leakage currents, while according to the SAED patterns (Figs. 3(a)–3(c) and 3(e)), microstructural quality varies from highly oriented films (AlN) to nm-sized domains in $Sc_{0.3}Al_{0.7}N$.

F. Piezoelectric properties

The PFM and DBI techniques were used to measure the converse piezoelectric response of the samples. The piezoelectric responses in pm/V for the samples with Sc concentration in the range of $0 \le x \le 0.3$ grown at $T_s = 400$ and 800 °C are shown in Figure 7(a). Comparison is made with theoretical predictions based on the results in Ref. 8, where e_{33} and c_{33}^E are derived, allowing to calculate the theoretical

Downloaded 19 Jun 2012 to 130.236.83.30. Redistribution subject to AIP license or copyright; see http://jap.aip.org/about/rights_and_permissions

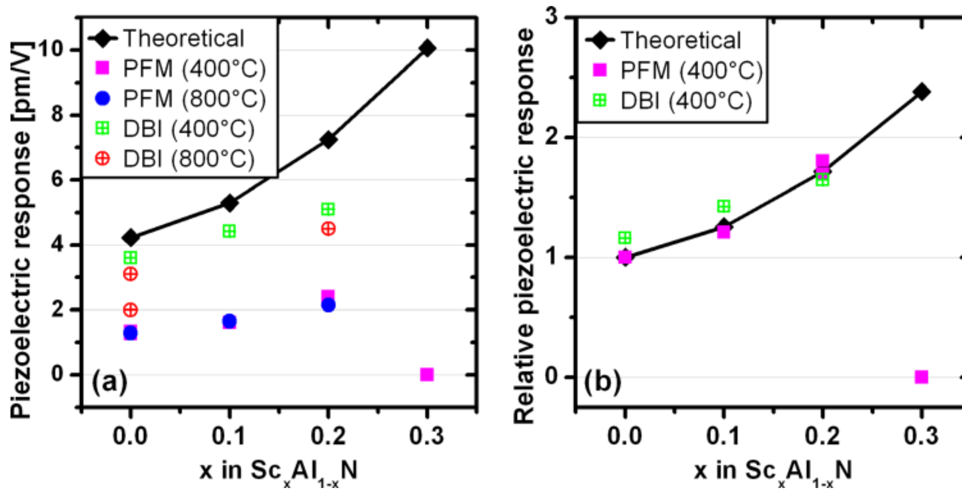

FIG. 7. Piezoelectric response in the films with different Sc concentrations: (a) as-measured and (b) relative response normalized to AlN response. Theoretical values are based on Ref. 8. PFM – piezo-force microscopy, DBI – double beam interferometry, substrate temperature is specified in the brackets.

values of the clamped thin film piezoelectric response $d_{33,f} = e_{33}/c^E_{33}$. Our AlN films show a response of ~1.3–3.6 pm/V, and up to 5 pm/V in piezoelectric response for Sc-containing samples with x = 0.2, depending on measurement technique. While this increase does not depend on growth temperature, it is noteworthy that $Sc_{0.2}Al_{0.8}N$ samples deposited at 800 °C have quite high leakage currents and the crystal structure is rather poor (Fig. 4(d)), while the microstructural quality, according to SAED pattern (inset in Fig. 3(d)) is comparable to the reference AlN (Fig. 3(b)). Noise level and fluctuations were higher in the 800 °C sample during the piezoelectric evaluation as compared to samples deposited at lower temperature. For samples with x = 0.3 grown at T_s = 400 °C, the piezoelectric response is equal to zero, while leakage current measurements indicate a dielectric material. The SAED pattern from this sample consists of arc-shaped spots indicating degradation in microstructure (inset in Fig. 3(e)) similar to $Sc_{0.3}Al_{0.7}N$ grown at 800 °C. This suggests that the influence of the microstructure is more important than crystalline quality for the piezoelectric properties of this material while the dielectric properties are affected in a different manner.

It is noted that the interferometer method has been extensively utilized for the characterization of ~2 μm thick textured AlN deposited at room temperature on Si substrates[25] where a typical high quality sample then shows a 5 pm/V response as compared to 3.6 pm/V in our sample and a theoretical value of 4.2 pm/V shown in Fig. 7(a). A common reason for lower piezoelectric response in AlN, despite having high level of orientation, is a non-homogenous polarization, due to for instance O contamination.[26] Phase response mapping done with the PFM method on the epitaxially grown AlN, however, did not reveal any domain misalignment. There is a lack of other comparable measurements done on reactively magnetron sputtered epitaxial AlN onto Al_2O_3 substrates. Any inherent property difference of such film and how the differences relate to the effective piezoelectric response, compared to the more common non-epitaxial AlN thin films on Si, remains to be investigated.

While the absolute values of d_{33} are different from non-epitaxial AlN as well as for the same samples analyzed with different techniques, the responses plotted on a relative scale (normalized to the AlN response for each technique) show a good correlation, also with the theoretical predictions reproduced from Ref. 8 (Fig. 7(b)). It is also noted that the relative increase in response with increased Sc concentration agrees well with the earlier reported results by Akiyama *et al.*[7] where 0.5–1.1 μm thick films on Si substrates were evaluated by a piezometer system. Our observations suggest that the absolute piezoresponse values should be treated carefully, while normalized values could be a way of comparing results obtained with different methods.

IV. CONCLUSIONS

Wurtzite $Sc_xAl_{1-x}N$ ($0 < x \leq 0.3$) thin films can be deposited from elemental Al and Sc targets using reactive magnetron sputtering in an Ar/N discharge onto $Al_2O_3(0001)$ substrates with a TiN(111) seed layer kept at 400–800 °C and at floating potential. By alloying AlN with ScN, the films experience degradation in both microstructural and crystalline quality with increasing concentration of Sc. Correspondingly, although the best quality AlN was obtained at 800 °C, all Sc-containing films grown at such high temperature exhibit leakage currents that increase with Sc concentration related to a deteriorating microstructure in terms of defect density as well as the apparent phase separations into Sc and Al rich domains.

By limiting the growth temperature to 400 °C, all films in the composition range possess negligible leakage currents and a true dielectric behavior. From a structural aspect, an increase in Sc content degrades the crystalline quality also at this lower temperature, though no phase separation could be detected. Films grown at temperatures lower than 400 °C show no improvement in crystal quality, most likely due to kinetic limitations for the crystal growth. Changing the seed layer to ZrN(111) gave little or no effect as well, probably due to increased surface roughness or lower ad-atom mobility.

The piezoresponse of the $Sc_xAl_{1-x}N$ films obtained by the PFM and DBI techniques revealed a consistent increase in magnitude with increasing Sc concentration up to x = 0.2, also in agreement with theoretical predictions from Ref. 8. The result was unaffected by the growth temperature, even though measurements performed on films deposited at 400 °C were more stable. The piezoelectric response was

Downloaded 19 Jun 2012 to 130.236.83.30. Redistribution subject to AIP license or copyright; see http://jap.aip.org/about/rights_and_permissions

maintained in all samples where SAED patterns confirmed good microstructure, while leakage current was low only in samples that, according to HRTEM and XRD analysis, had high crystalline quality.

ACKNOWLEDGMENTS

The PFM measurements were performed at Max Planck Institute of Microstructure Physics in Halle, Germany. The authors are thankful to Dr. Marin Alexe and Professor Dietrich Hesse for useful discussions and valuable advice.

We acknowledge the Swedish Research Council and European Research Council as well as Swedish Foundation for Strategic Research for support of this study.

[1]M. Reine, P. Lamarre, and A. Hairston, Compound Semicond. **12**, 5 (2006).
[2]J. Wu, J. Appl. Phys. **106**, 1 (2009).
[3]A. Hörling, L. Hultman, M. Odén, J. Sjölén, and L. Karlsson, Surf. Coat. Technol. **191**, 2–3 (2005).
[4]L. Rogström, L. J. S. Johnson, M. P. Johansson, M. Ahlgren, L. Hultman, and M. Odén, Scr. Mater. **62**, 10 (2010).
[5]F. Bernardini, V. Fiorentini, and D. Vanderbilt, Phys. Rev. B **56**, 16 (1997).
[6]R. Aigner, Sens. Update **12**, 1 (2003).
[7]M. Akiyama, T. Kamohara, K. Kano, A. Teshigahara, Y. Takeuchi, and N. Kawahara, Adv. Mater. **21**, 5 (2009).
[8]F. Tasnádi, B. Alling, C. Höglund, G. Wingqvist, J. Birch, L. Hultman, and I. A. Abrikosov, Phys. Rev. Lett. **104**, 13 (2010).
[9]C. Höglund, J. Birch, B. Alling, J. Bareño, Z. Czigány, P. O. Å. Persson, G. Wingqvist, A. Zukauskaite, and L. Hultman, J. Appl. Phys. **107**, 12 (2010).
[10]G. Wingqvist, F. Tasnádi, A. Zukauskaite, J. Birch, H. Arwin, and L. Hultman, Appl. Phys. Lett. **97**, 11 (2010).
[11]M. Moreira, J. Bjurström, I. Katardjev, and V. Yantchev, Vacuum **86**, 1 (2011).
[12]R. Matloub, A. Artieda, C. Sandu, E. Milyutin, and P. Muralt, Appl. Phys. Lett. **99**, 9 (2011).
[13]M. Akiyama, K. Kano, and A. Teshigahara, Appl. Phys. Lett. **95**, 16 (2009).
[14]J. C. Schuster and J. Bauer, J. Less-Common Met. **109**, 2 (1985).
[15]C. Höglund, J. Bareño, J. Birch, B. Alling, Z. Czigány, and L. Hultman, J. Appl. Phys. **105**, 11 (2009).
[16]T. Bohnen, G. R. Yazdi, R. Yakimova, G. W. G. van Dreumel, P. R. Hageman, E. Vlieg, R. E. Algra, M. A. Verheijen, and J. H. Edgar, J. Cryst. Growth **311**, 11 (2009).
[17]J. A. Christman, R. R. Woolcott, A. I. Kingon, and R. J. Nemanich, Appl. Phys. Lett. **73**, 26 (1998).
[18]M. Alexe and A. Gruverman, *Nanoscale Characterization of Ferroelectric Materials: Scanning Probe Microscopy Approach* (Springer, Berlin, 2004).
[19]A. L. Kholkin, C. Wütchrich, D. V. Taylor, and N. Setter, Rev. Sci. Instrum. **67**, 5 (1996).
[20]A. Artieda, C. Sandu, and P. Muralt, J. Vac. Sci. Technol. A **28**, 3 (2010).
[21]V. Stambouli, O. Burat, D. Bouchier, F. Meyer, J.-P. Gilles, and G. Gautherin, Thin Solid Films **193–194**(part 1), 181–188 (1990).
[22]D. W. Hoffman and J. A. Thornton, J. Vac. Sci. Technol. **20**, 3 (1981).
[23]H. F. Winters and E. Kay, J. Appl. Phys. **38**, 10 (1967).
[24]F. Engelmark, J. Westlinder, G. F. Iriarte, I. V. Katardjiev, and J. Olsson, IEEE Trans. Electron Devices **50**, 5 (2003).
[25]F. Martin, P. Muralt, M. A. Dubois, and A. Pezous, J. Vac. Sci. Technol. A **22**, 2 (2004).
[26]M. Akiyama, T. Kamohara, K. Kano, A. Teshigahara, and N. Kawahara, Appl. Phys. Lett. **93**, 2 (2008).

Downloaded 19 Jun 2012 to 130.236.83.30. Redistribution subject to AIP license or copyright; see http://jap.aip.org/about/rights_and_permissions